PLOS COMPLEX SYSTEMS

RESEARCH ARTICLE

Heavy-tailed jumps induce intermittent patterns and gradual transitions in interacting cell populations

Josué Manik Nava-Sedeño*

Mathematics Department, Sciences Faculty, Universidad Nacional Autónoma de México, Ciudad Universitaria, Mexico City, Mexico

* manikns@ciencias.unam.mx

Abstract

It has been widely accepted, that a key step in cancer invasion and metastasis is the so-called epithelial-mesenchymal transition (EMT), where cells lose contacts with their neighbors and start moving freely, colonizing new tissues in the process. However, it has been found that cancer cells may retain cellular contacts and become highly metastasizing without undergoing EMT. Furthermore, single cancerous cells may reach far away tissues by displaying superdiffusive Lévy dynamics. Here, we study a system of collectively migrating cells with attracting (adhesive) interactions and heavy-tailed distributed jump lengths. To this end, we develop a multi-speed lattice-gas cellular automaton model, and analyze it both computationally and analytically. To study the effect of Lévy dynamics on collective behavior, we consider three migration scenarios: (classic) single-jump migration, corresponding to a "healthy" scenario, where cells move a single site per time step, block migration, where cells that move together remain together for the total duration of the jump but jump lengths are random and power-law distributed, corresponding to the case where leader cells can guide cell clusters through strong cell junctions, and cell-wise migration, where each cell in a group may perform jumps of different lengths, independently of other cells, corresponding to the case where cell junctions are dynamic enough to allow single cells to escape clusters. We show that, while in the classic case, destabilization of the homogeneous steady state only depends on cell density and/or adhesion strength, in the multi-speed case, increasing the probability of long jump lengths leads to a gradual order-disorder transition, as opposed to the sharp transition with increasing cell density and/or adhesiveness. Furthermore, observed spatial patterns formed are stable when jumps are preferentially small, unstable when long jumps are highly probable, and metastable at intermediate regimes.

OPEN ACCESS

Citation: Nava-Sedeño J M. (2025) Heavy-tailed jumps induce intermittent patterns and gradual transitions in interacting cell populations. PLoS Complex Sys 2(6): e0000048. https://doi.org/10.1371/journal.pcsy.0000048

Editor: John Edward Green, The University of Adelaide - North Terrace Campus: The University of Adelaide, AUSTRALIA

Received: October 14, 2024

Accepted: April 20, 2025

Published: June 2, 2025

Peer Review History: PLOS recognizes the benefits of transparency in the peer review process; therefore, we enable the publication of all of the content of peer review and author responses alongside final, published articles. The editorial history of this article is available here: https://doi.org/10.1371/journal.pcsy.0000048

Data availability statement: The code used for producing the simulation results reported in the

manuscript can be freely accessed at https://github.com/tailswalker/Zeta-adhesive.

Funding: The author(s) received no specific funding for this work.

Competing interests: The author has declared that no competing interests exist.

Author summary

Living organisms, as well as some man-made objects, move while influencing the movement of one another along the way, in what is referred to as collective migration. Much research has focused on the effect of particular types of individual interactions on the formation of patterns at the population level. For example, attractive interactions (also called adhesive in the cellular context), promote the formation of groups with a large number of individuals. Most models, however, assume that when isolated, individuals will move a small distance in a fixed time window. However, current research has found that some cells perform "Lévy movement", a type of movement where cells tend to move great distances, even when their direction may be random. In this work, we construct a model to study a system of individuals with attractive interactions, but which may randomly move very far away individually. We find that group formation can still happen, as long as large displacements are not too frequent, and that high odds of large displacements coupled to high attractive strength may result in the formation of short-lived clusters, rather than stable clusters.

Introduction

Several biological systems [1–4], as well as some artificial ones including robot swarms [5] and active colloids [6], consist of individuals which use energy to propel themselves, and when close enough to one another, may interact in some way to affect each other's behavior. Commonly, it is assumed that individuals in isolation perform random walks and diffuse normally. The study of such systems generally falls under the field of "active matter" [7,8].

In the particular case of groups of biological cells, interactions may result in the coordinated movement of individuals in a defined direction [9], or alignment of their body shape [10], to name a few. Animal cells, for example, interact strongly through attractive, or adhesive, interactions, caused by the presence of molecules such as cadherins [11]. Under physiological conditions, cells adhere strongly and form stable tissues and other structures. It is generally accepted that cells which become malignant become less adhesive, and thus can escape their original tissue to colonize other far away regions during the metastatic cancer phase [12], undergoing what is known as epithelial-mesenchymal transition, or EMT[13]. Additionally, it has been recently found that metastatic cells may not only have a decreased adhesiveness, but also behave superdiffusively in isolation [14,15], meaning that they tend to move further distances than normally diffusive cells. Furthermore, some metastatic cell populations may be significantly more invasive when their adhesiveness is high, and remain in cell clusters, than when their adhesiveness is low, and move as individual cells [16], as highly motile cells may carry other tumor cells along through intact cell junctions [17].

Though collective migration, pattern formation, cluster formation, and self-organization has been actively studied using a plethora of mathematical models, so far most models assume cells perform random walks or Brownian motion when cell-cell interactions are absent [18–22]. The study of active matter with Lévy flight-like movement dynamics has only started to be studied recently [23–29], and, to the best of our knowledge, has never been considered in combination with attractive interactions. In some cases, the study of such systems skips the microscopic, individual-level description, and instead consider a macroscopic, partial-differential equation (PDE) model, where the effect of the individual-level superdiffusive dynamics is assumed to simply result in the exchange of local differential operators for non-local fractional pseudodifferential operators (see for example [30]).

In this work, we study the effects of non-Brownian jump dynamics in a population of interacting cells, by comparing the behavior of a population of adhesive cells with power-law distributed jump lengths, to that of of a population of equally interacting cells, but whose jump lengths are constant, thus performing a random walk in isolation. We start by defining a discrete lattice-gas cellular automaton (LGCA) model with random jump lengths in one dimension, which is akin to heavily confined cells in a stiff extracellular matrix. Afterward, we derive a mean-field, macroscopic description of the system which we analyze both analytically and numerically, to theoretically predict the behavior of the model with respect to cell density, adhesion sensitivity, and jump-length distribution parameters. Finally, we corroborate our theoretical results using computer simulations, and we discuss the spatio-temporal patterns observed in our simulations.

Materials and methods

Model definition

We model the system of adhesive cells by a lattice-gas cellular automaton. Like all true cellular automata, the LGCA consists of a discrete spatial lattice $\mathcal{L}$, a discrete state space $\mathcal{E}$, a local neighborhood $\mathcal{N}$, and a local rule $\mathcal{R}$ [31].

Spatial lattice $\mathcal{L}$. For simplicity, we consider a one-dimensional lattice $\mathcal{L} \subset \mathbb{Z}$. Due to computational restraints, we consider a finite lattice $\mathcal{L} = \{0, 1, 2, \ldots, L - 1\}$. Cells can only be located within lattice nodes $r \in \mathcal{L}$. Unlike regular cellular automata, nodes in LGCA posses a substructure: every node has exactly two velocity channels, $c_1 = 1$, $c_2 = -1$. Cells moving to the right are said to occupy channel c_1, while cells moving to the left occupy channel c_2.

State space $\mathcal{E}$. Traditionally, channels can be occupied by one cell at most, which introduces an exclusion principle. In this work, we instead use an exclusion-free LGCA extension [32]. Thus, channel occupation, $s_j(r,k) \in \mathbb{N}_0, j \in \{1,2\}$ indicates how many cells are located within the velocity channel c_j at node r at time step k, i.e. how many cells in the node are moving in a certain direction, and any number of cells can move in the same direction at the same spatial location. Thus, the state of a node r at time step k is given by

$$\mathbf{s} \in \mathcal{E} := \mathbb{N}_0^2.$$

Note that the total number of cells in a node, irrespective of their direction of motion, is given by

$$n[\mathbf{s}(r,k)] = \sum_{j=1}^{2} s_j(r,k).$$

Neighborhood $\mathcal{N}$. The neighborhood of a node $r \in \mathcal{L}$ is a subset of the lattice $\mathcal{L}$, such that only cells within this interaction neighborhood can affect the behavior of cells at r. In this case, we consider only the first neighbors of r. Furthermore, since the lattice used for simulations is finite, we define periodic boundary conditions. Therefore, the interaction neighborhood of the node $r \in \mathcal{L}$ is defined as

$$\mathcal{N}_r := \{r + c_1 (\mathrm{mod}\, L), r + c_2 (\mathrm{mod}\, L)\}.$$

Rule $\mathcal{R}$. In cellular automata, time advances in discrete time steps $k \in \mathbb{N}$. A rule $\mathcal{R}$ is applied to every node in the lattice simultaneously, which changes the state of every node to a new state, after which we consider that a single time step has elapsed. In LGCA, the rule consists of two sequential steps, the interaction step $\mathcal{I}$, followed by the migration step $\mathcal{M}$. We

will not consider cell birth/death, thus the interaction step rearranges cells within velocity channels without changing the number of cells per node.

The interaction step models the change in the cells' direction of motion due to adhesive interactions. We assume that the probability that a single cell occupies a certain velocity channel is independent of the velocity channel occupation of other cells within the same node. Then, the probability that a cell occupies the j-th velocity channel after the interaction step is

$$W_j(r,k) = \frac{1}{Z}\exp\left[\beta c_j G(r,k)\right], \tag{1}$$

where Z is the normalization constant, $\beta \in \mathbb{R}_+$ is called the sensitivity, which controls the randomness of the interaction, and the local discrete adhesive gradient is given by

$$G(r,k) = \sum_{j=1}^{2} c_j n\left[\mathbf{s}\left(r + c_j, k\right)\right],$$

which points in the direction of maximum cell density. Note that, when $\beta = 0$, states $\mathbf{s}$ change uniformly among all states with the same number of cells as in the original state, while in the limit $\beta \to \infty$, states change deterministically to the state where the cell's velocity forms the minimum angle with respect to the adhesive gradient. Furthermore, the transition probability is uniform, irrespective of β, whenever the adhesive gradient vanishes.

We consider three different migration modes. First, as in traditional LGCA, the migration step is deterministic, and cells move to the nearest neighboring node in the direction of the velocity channel they occupy after interaction. We refer to this mode of migration 'single step'. Additionally, we consider a multi-velocity extension, where cells move in the direction of their velocity channel, but into a node at a random distance M away from the original node. To model the possibility that cells travel very long distances, we define M as a Zeta-distributed random variable, with probability mass function (pmf) given by

$$p_M(m) = \frac{m^{-s}}{\zeta(s)},\ m \in \mathbb{N}, \tag{2}$$

where $\zeta(s)$ is the Riemann zeta function, which is the distribution's normalization constant, and the parameter $s>1$ is inversely proportional to the weight of the distribution's tail. The Zeta distribution was selected because power-law-distributed displacements ($f(m) \propto m^{-s}$) have been observed in the motility of several cell types[14,33,34]. Additionally, the Zeta distribution incorporates the exponent s as a tunable parameter, enabling the systematic study of the effect of varying jump lengths on collective behavior. While continuous heavy-tailed distributions, such as the Lévy distribution, have been employed in prior studies, the discrete nature of our model necessitates a discrete heavy-tailed distribution, for which the Zeta distribution is the most widely recognized. We consider two cases for the multi-velocity migration step:

- Cell-wise jumps. In this case, each cell within a velocity channel chooses a node to land into, following Eq (2), independently of all other cells.
- Block migration. In this case, all cells within the same channel move into the same node, according to Eq (2).

The full dynamics of the LGCA with block migration can be summarized as a stochastic finite difference equation, known as the microdynamical equation, which reads

$$s_j(r, k+1) = s_j^{\mathcal{I}}(r - Mc_j, k), \tag{3}$$

where $s_j(r,k)$ and $s_j^{\mathcal{I}}(r,k)$ are the occupation of the j-th channel before and after interaction, respectively, of node r at time step k. This equation states that cells occupying the j-th velocity channel at the next time step, are cells that occupy the same channel at the current time step, after the interaction step has changed cell velocities, a distance M away, traveling in the direction of their velocity channel, as seen in Fig 1.

Computational implementation

The lattice size was set at $L = 300$ nodes, which allowed to maintain computational efficiency while enabling a proper sampling of the long displacements introduced by the Zeta distribution. Periodic boundary conditions were used in all cases. To simulate a disordered, spatially homogeneous initial condition, each velocity channel of every lattice node was assigned a single particle randomly following a binomial process with probability $\bar{f} \in (0,1)$. To characterize the degree of aggregation of cells, we measured the spatial entropy after 500 time steps had elapsed, defined as

$$S(k) = -\sum_{r\in\mathcal{L}} \frac{n[\mathbf{s}(r,k)]}{N_{\text{tot}}} \ln\left\{\frac{n[\mathbf{s}(r,k)]}{N_{\text{tot}}}\right\}, \tag{4}$$

where

$$N_{\text{tot}} = \sum_{r\in\mathcal{L}} n[\mathbf{s}(r,k)]$$

is the total number of cells in the entire lattice. When cells are uniformly distributed among all nodes, entropy reaches its maximum value $S_{\max} = \ln L$.

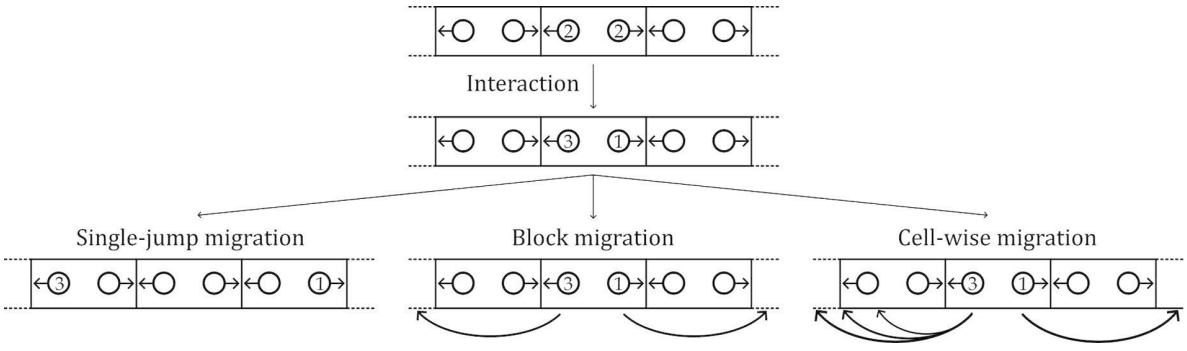

Fig 1. Dynamics of the multi-velocity LGCA. During the interaction step $\mathcal{I}$, cells change their velocities stochastically according to Eq (1), occupying new velocity channels within their original node. Afterwards, during the migration step $\mathcal{M}$, we consider three migration modes. 1. Single-jump migration: All cells within a channel are transported into the same channel in the neighboring node in the direction of the velocity channel. 2. Block migration: All cells within a channel are transported into the same channel in a node a random distance M away, distributed as Eq (2), in the direction of the velocity channel. 3. Cell-wise migration: Every cell is transported to a different random node M sites away, in the direction of their velocity channel. The time step number is increased after the interaction and migration steps have been applied to every node in the lattice simultaneously.

https://doi.org/10.1371/journal.pcsy.0000048.g001

Results

Mathematical analysis in the local case

First, we consider single-step migration. To analyze this case, we start with Eq (3), setting $M = 1$. Next, we calculate the expected value of this equation conditioned to $\mathcal{F}_k$, the filtration of the stochastic process up to time step k, which yields

$$\left\langle s_j(r, k+1) \mid \mathcal{F}_k \right\rangle = n\left[\mathbf{s}\left(r - c_j, k\right)\right] W_j\left(r - c_j, k\right),$$

since the interaction step is binomial due to the independence between cells in the same node during interaction. Now, we take the total expected value of the previous expression. We use a mean-field approximation, which considers that the effect of cell interactions on any cell can be approximated by the effect of the average cell interaction on the cell. Mathematically, this approximation considers that all cell variables are independent random variables with zero standard deviation. Therefore, for any function F, we may approximate $\langle F[\mathbf{s}_{\mathcal{L}}(k)]\rangle \approx F[\langle \mathbf{s}_{\mathcal{L}}(k)\rangle]$. Such an approximation results in

$$f_j(r, k+1) = \left\langle n\left[\mathbf{s}\left(r - c_j, k\right)\right]\right\rangle P_j\left(r - c_j, k\right),$$

where $P_j(r, k)$ is the mean-field channel occupation probability

$$P_j(r, k) = \frac{1}{Z} \exp\left\{\beta c_j \sum_{\ell=1}^{2} c_\ell \left\langle n\left[\mathbf{s}\left(r + c_\ell, k\right)\right]\right\rangle\right\}, \tag{5}$$

and $f_j(r, k) = \left\langle s_j(r, k)\right\rangle$ is the mean occupancy of the j-th velocity channel of node r at time step k. Afterward, we add over j and denote by

$$u(r, k) = \langle n[\mathbf{s}(r, k)]\rangle = \sum_{j=1}^{2} f_j(r, k)$$

the expected number of cells in node r at time step k, and obtain the finite difference equation

$$u(r, k+1) = u(r-1, k)P_1(r-1, k) + u(r+1, k)P_2(r+1, k). \tag{6}$$

We could perform the analysis on this discrete equation; however, we will instead derive an approximate partial differential equation, and analyze the model's dynamics at the continuous level.

To this end, we now rescale the time by a constant time step length, $\tau > 0$, and a constant lattice spacing $\varepsilon > 0$. We define the continuous time and space variables $t = k\tau$ and $x = r\varepsilon$, respectively and, using that $P_1(r, k) + P_2(r, k) = 1$,we obtain the equation

$$u(x, t+\tau) = u(x-\varepsilon, t) - u(x-\varepsilon, t)P_2(x-\varepsilon, t) + u(x+\varepsilon, t)P_2(x+\varepsilon, t).$$

Now, we perform a Taylor series expansion up to first order in t, and up to second order in x. We define the cell speed $v = \frac{\varepsilon}{\tau}$ and diffusion constant $D = \frac{\varepsilon^2}{2\tau}$ to obtain the approximate partial differential equation

$$\frac{\partial}{\partial t} u = D \frac{\partial^2}{\partial x^2} u + v \frac{\partial}{\partial x}\left(2uP_2 - u\right), \tag{7}$$

where the discrete adhesive gradient becomes the continuous gradient and therefore the channel occupation probability can be written as

$$P_2(x,t) = \frac{1}{2}\exp\left[-2\tilde{\beta}\frac{\partial}{\partial x}u(x,t)\right]\operatorname{sech}\left[2\tilde{\beta}\frac{\partial}{\partial x}u(x,t)\right],$$

where we have expanded the normalization constant Z, and $\tilde{\beta} = \varepsilon\beta$.

The spatially homogeneous steady state, $u(x,t) = \bar{u}$, $\bar{u} \in \mathbb{R}\ \forall t, x \in \mathbb{R}$ (or equivalently, $f(x,t) = \bar{f}, \bar{f} = \frac{\bar{u}}{2}$) is an equilibrium solution of Eq (7), since in this case $P_2 = \frac{1}{2}$ and all derivatives vanish. Since the PDE is nonlinear in both u and $\frac{\partial}{\partial x}u$, we linearize around the homogeneous steady state to obtain

$$\frac{\partial}{\partial t}u = (D - 4D\beta\bar{u})\frac{\partial^2}{\partial x^2}u, \tag{8}$$

which is just the diffusion equation with diffusion constant $D - 4D\beta\bar{u}$. Thus, cells stop spreading and start aggregating when the diffusion constant becomes negative, i.e. when

$$\beta\bar{u} > \frac{1}{4}. \tag{9}$$

Therefore, the model predicts spontaneous aggregation if either the sensitivity or cell density are sufficiently high, where both sensitivity and cell density contribute equally to the instability of the homogeneous steady state. These results agree with previous research on cell populations with adhesive interactions [35,36].

Mathematical analysis in the non-local case

In the case of Zeta-distributed jumps, we restrict ourselves to the block-migration case, due to ease of analysis, and since the qualitative differences between both cases are mostly restricted to jump distributions with extremely heavy tails and low cell-cell interaction strength.

We start by finding the continuous PDE similarly to the single jump case, following [37]. We use Eq (3) and the total expected value, as well as a mean-field approximation as before. However, due to the random jump lengths, we obtain

$$f_j(r,k+1) = \sum_{m=1}^{\infty} u(r - mc_j, k)P_j(r - mc_j, k)p_M(m), \tag{10}$$

where $p_M(m)$ is the probability mass function of the Zeta-distributed jump length, given by Eq (2). Adding over n, rescaling time and space, subtracting $u(x,t)$ on both sides of the equality, and using probability axioms, we obtain

$$\begin{aligned} u(x,t+\tau) - u(x,t) = \sum_{m=1}^{\infty} p_M(m)\,[&P_1(x - m\varepsilon, t)u(x - m\varepsilon, t) \\ &+P_2(x + m\varepsilon, t)u(x + m\varepsilon, t) - u(x,t)]\,. \end{aligned}$$

We again use that $P_1+P_2=1$, we add a zero to the right-hand side of the equation, and rearrange, to obtain

$$\begin{aligned}u(x,t+\tau)-u(x,t)&=\sum_{m=1}^{\infty}p_M(m)\left[u(x-m\varepsilon)-u(x,t)\right]\\&-\sum_{m=1}^{\infty}p_M(m)\left[-P_2(x+m\varepsilon,t)u(x+m\varepsilon,t)+2P_2(x,t)u(x,t)-P_2(x-m\varepsilon,t)u(x-m\varepsilon,t)\right]\\&+2\sum_{m=1}^{\infty}p_M(m)\left[P_2(x,t)u(x,t)-P_2(x-m\varepsilon,t)u(x-m\varepsilon,t)\right].\end{aligned}$$

Now, we substitute Eq (2), define the new constant $s'=\frac{s-1}{2}\in[0,\infty)$ since $s\in[1,\infty)$, divide everywhere by τ, multiply and divide the right hand side by $\varepsilon^{2s'}$, and multiply and divide the second term in the right hand side by two, so that for small τ and ε, the equation is approximated by the integro-differential, fractional PDE

$$\begin{aligned}\frac{\partial}{\partial t}u(x,t)=D_1\int_0^{\infty}\frac{u(x-y,t)-u(x,t)}{y^{2s'+1}}\mathrm{d}y-2D_2\left(-\Delta\right)^{s'}_{\mathbb{R}_+}\left[P_2(x,t)u(x,t)\right]\\+2D_1\int_0^{\infty}\frac{P_2(x,t)u(x,t)-P_2(x-y,t)u(x-y,t)}{y^{2s'+1}}\mathrm{d}s,\end{aligned}\tag{11}$$

where the constants are defined as

$$\begin{aligned}D_1&=\frac{\varepsilon^{2s'}}{\tau\zeta(2s'+1)},\\D_2&=\frac{\varepsilon^{2s'}}{\tau\zeta(2s'+1)c_{1,s'}},\end{aligned}$$

and $c_{1,s'}$ is the fractional Laplacian proportionality constant [38], and the censored fractional Laplacian is defined as [37]

$$\left(-\Delta\right)^{s'}_{\mathbb{R}_+}f(x)=\frac{c_{1,s'}}{2}\int_0^{\infty}\frac{2f(x)-f(x+y)-f(x-y)}{y^{2s'+1}}\mathrm{d}y.\tag{12}$$

Since the nonloncal terms (with the exception of the censored fractional Laplacian) do not correspond to pseudodifferential operators, the analysis of the solutions to Eq (11) is difficult to perform analytically. Thus, to analyze the model, rather than focusing on the continuous approximation Eq (11) as done previously, for simplicity we instead turn to the mean-field, discrete, finite difference equation. We start by considering Eq (10), noting that, due to the normalization of the probabilities $p_M(m)$ and $P_n(r,k)$, the disordered, spatially homogeneous steady state $f_n(r,k)=\bar{f}=\frac{\bar{u}}{2}\ \forall k\in\mathbb{N}$, $r\in\mathcal{L}$, $n\in\{1,2\}$, $\bar{f}\in\mathbb{R}_+$, is a solution to Eq (10). We linearize the equation around this steady state and, using the definition of the mean-field probabilities Eq (5), the linearized system reads

$$\begin{aligned}&f_j(r,k+1)=\\&\sum_{m=1}^{\infty}\frac{1}{2}p_M(m)\sum_{\ell=1}^{2}f_\ell(r-mc_j,k)+\beta\bar{u}c_j\left[f_\ell(r-mc_j+1,k)-f_\ell(r-mc_j-1,k)\right].\end{aligned}$$

Finally, we perform a discrete Fourier transform, using the shift theorem

$$\mathfrak{F}\left\{X_{r+m}\right\}(q) = e^{iqm}\mathfrak{F}\left\{X_r\right\}(q),$$

where $q = \frac{2\pi\omega}{L}$, $\omega \in \{0, 1, \ldots, L-1\}$, and recalling the definition of the characteristic function of the random variable M,

$$\phi_M(y) = \sum_{m=1}^{\infty} e^{iym} p_M(m),$$

we obtain the linear FDE system

$$\hat{\mathbf{f}}(k+1) = \Gamma(q)\hat{\mathbf{f}}(k),$$

where the matrix Γ is called the Boltzmann propagator, whose entries are given in this case by

$$\Gamma_{j,\ell}(q) = \frac{\phi_M\left(-qc_j\right)}{2}\left(1 + 2i\beta\bar{u}c_j \sin q\right). \tag{13}$$

In this case, time is discrete and the number of cells is conserved, and thus the spatially homogeneous, disordered steady state is stable if and only if all eigenvalues $\lambda(q)$ of the Boltzmann propagator are such that $|\lambda(q)| \leq 1$ for all $q \in [0, 2\pi)$. Therefore, patterns with spatial wavelength $\frac{2\pi}{q}$ grow exponentially as $|\lambda(q)|^k$ if $|\lambda(q)| > 1$.

Since the the entries of the Boltzmann propagator do not depend on ℓ, its columns are not linearly independent, thus one eigenvalue is $\lambda_1 = 0\ \forall q \in [0, 2\pi)$. This eigenvalue predicts the almost instantaneous decay of modes with different channel occupation within a single node [39], since the adhesive interaction does not promote velocity polarization, but rather enhances the formation of regions with high cell density.

Note that, when we have single-step migration, $M = 1$, and its characteristic function is simply $\phi_M(q) = e^{iq}$, the second eigenvalue has a closed, real form

$$\lambda_2 = \cos(q) + 2\beta\bar{u}\sin^2(q). \tag{14}$$

Differentating and equating to zero, we find that it always has two extrema, one at $q = 0$ where $\lambda_2 = 1$, corresponding to mass conservation, and another at $q = \pi$ where $\lambda_2 = -1$, corresponding to a checkerboard artifact due to lattice regularity. However, when $\beta\bar{u} > \frac{1}{4}$, λ_2 has another maximum greater than one, which destabilizes the spatially uniform steady state. This agrees with the result obtained from the linearization of the PDE approximation in the single-step migration case.

In the long-jump case, the remaining eigenvalue spectra λ_2 depends on the Zeta distribution parameter, s, as well as on the product of the interaction sensitivity β and $\bar{u}$, as in the single-jump case. This means that, linearly, changes in β have the same effect as changes in $\bar{u}$.

While the non-trivial eigenvalue spectra in the single-jump and long-jump cases are qualitatively very similar in the low sensitivity, low density regime, important differences arise when considering the strongly interacting and/or high density cases. As seen in Fig 2, in the highly adhesive case, the dominant wavenumber q corresponding to the global maximum of the eigenvalue spectrum, $\lambda(q)$, does not change noticeably between the short and long jump cases. Therefore, the wavelength of emergent spatial patterns is largely consistent, independently of jump lengths. However, the height of the maximum does decrease monotonically with decreasing s, dipping well below the $|\lambda| = 1$ mark for low enough values of s. Thus, while

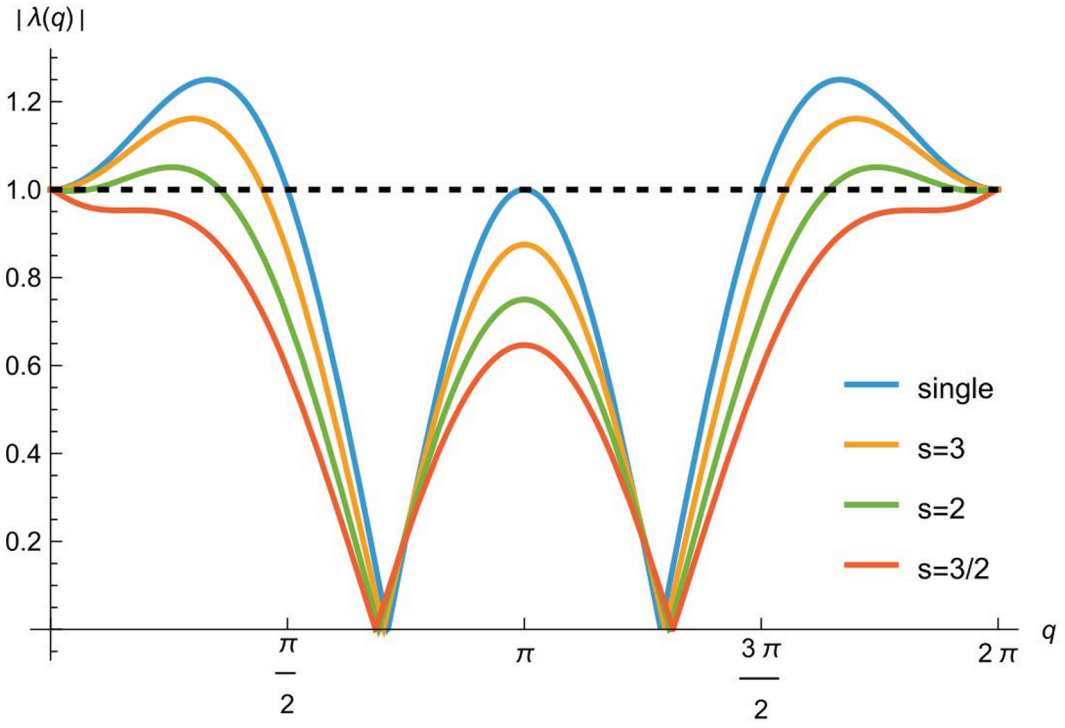

Fig 2. Eigenvalue spectra for Zeta-distributed jump lengths. The spectra shown were calculated numerically for $\beta\bar{u} = \frac{1}{2}$. The blue line corresponds to the single-jump case, where the eigenvalue spectrum is given by Eq (14). Other colors correspond to spectra corresponding to the non-trivial eigenvalue of Eq (13), with $s = 3$ (yellow line), $s = 2$ (green line), and $s = \frac{3}{2}$ (red line). The characteristic function of the Zeta distribution was used in these cases. The critical value, $|\lambda| = 1$ is shown as a dashed line. As long jumps become more probable (deceasing s), the rate of divergence from the steady state $\lambda(q)$ decreases. The steady state becomes linearly stable at sufficiently low values of s when $|\lambda(q)| \leq 1 \forall q \in [0, 2\pi)$.

https://doi.org/10.1371/journal.pcsy.0000048.g002

patterns may still form when long jumps become increasingly more probable, they do so more slowly, and stop forming altogether once the tails of the jump distribution become too heavy.

Computer simulations

We performed computer simulations of the model with all three migration modes, and compared the results with the theoretical predictions discussed earlier.

First, we performed a parameter sweep, varying both the sensitivity β, and the mean initial channel occupation $\bar{f} = \frac{\bar{u}}{2}$ of the initially homogeneous steady state, with fixed jump distribution parameter $s = 6$. This value was chosen such that long jumps are probable enough to have a substantial impact in the dynamics of the model, but not so common that patterns are destroyed, as found theoretically. We measured the global entropy (Eq (4)) after simulating the model for 500 time steps, and averaged over 50 realizations. We find that the order-disorder transition for both cell-wise and block migration modes roughly follow the hyperbolic profile Eq (9) predicted theoretically for the single-jump migration mode (see Fig 3a and 3b). This suggests that the instability threshold resulting from Eq (13) with $\phi_M(s)$ corresponding to the Zeta distribution would be qualitatively similar to that of the single-jump case, so long jumps do not significantly affect the critical sensitivity and density values at the transition.

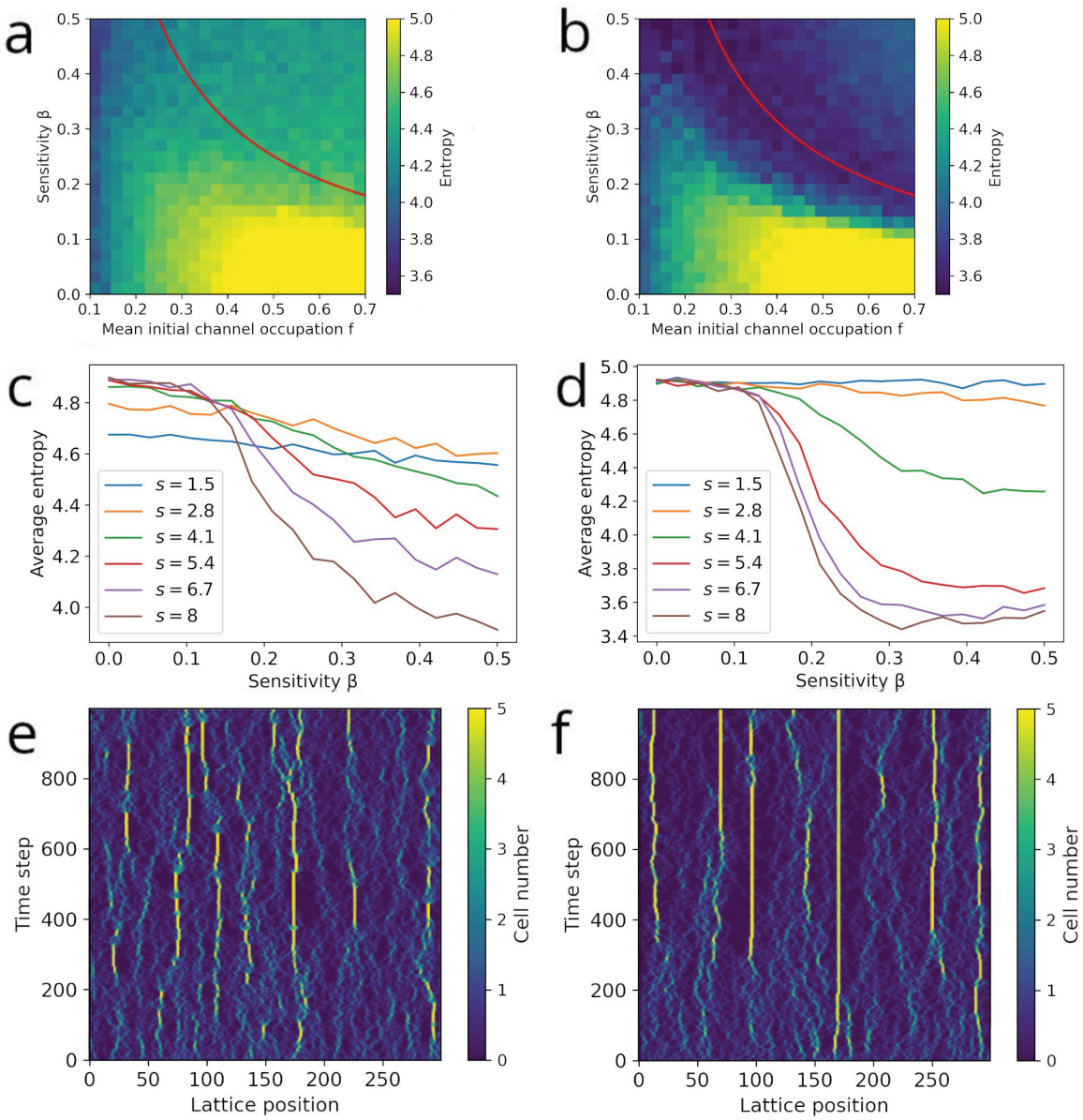

Fig 3. Simulations of the model with block (left column) and cell-wise (right column) migration. (a,b): Global spatial entropy (Eq (4)) for varying β and $\bar{f}$. The Zeta distribution parameter was fixed at $s = 6$. The color bar indicates the value of the entropy. The red line indicates the stability threshold given by Eq (9) for the classic single-jump case. (c,d): Global spatial entropy as a function of sensitivity β for several values of s. The mean initial channel occupation was set at $\bar{f} = 0.34$. As long jumps become less probable, the phase transition becomes steeper. (e,f): Kymographs (spatiotemporal plots) of single model realizations. The color bar indicates the total number of cells at node r at time step k, $n[\mathbf{s}(r,k)]$. Parameter values were set at $\bar{f} = 0.34$, $\beta = 0.25$, and either $s = 6$ (e) or $s = 5$ (f). In both cases, cell aggregates constantly break down and reform. In the cell-wise migration case, aggregates appear more long-lived than in the block migration case. Average entropy values were obtained by averging 50 model realizations.

https://doi.org/10.1371/journal.pcsy.0000048.g003

Then, we fixed $\bar{f} = 0.34$, and varied both β and s, and observed the mean entropy (see Fig 3c and 3d). First, we observe that, in both cases, the entropy profile is practically identical to that of the single-jump case for $s \approx 8$. Second, in both cases, the critical β value does not change significantly for varying s. However, the entropy of the ordered state steadily increases with decreasing s, until the transition is barely noticeable at $s \approx 2.8$. This indicates that long jumps

increase the global spatial disorder of cells, up to a point where cell-cell adhesion cannot prevent spatial disorder, independently of the adhesive strength. Finally, we notice that entropy in the block migration case reaches lower values than in the cell-wise migration case, even in the low-adhesion regime. This is to be expected, since even groups of cells which are located in the same velocity channel out of complete chance, will be forced to remain together during the migration phase, maintaining the spatial entropy at lower levels.

We also observed the spatial patterns formed in individual model realizations for high adhesiveness β and moderate odds for long jumps (intermediate values of s), to make sense of the higher values of the entropy after the transition discussed earlier. As observed in Fig 3e and 3f, for both block migration and cell-wise migration modes, aggregation patterns at these highly adhesive, highly motile regimes do not longer form and remain stable and stationary. Rather, cells start aggregating at high-density zones, and then randomly dissociate after some time, and reassemble at a different spatial point, and so on and so forth. Thus, at these parameter regimes, patterns form intermittently and are metastable. This behavior may be due to cells within an aggregate suddenly leaving and destroying it when randomly performing a long jump. This may also explain why aggregation patterns in the cell-wise migration case are more long lived than in the block migration case: the loss of a few cells performing long jumps is less deleterious than the loss of a big group of cells moving together to a node far away.

Robustness and generalizations of the model

To assess the robustness and generality of our model, we explored the dependence of the model's behavior on dimensionality, lattice geometry, and the number of neighbors. Additionally, we compared our model to an analogous non-local PDE model to highlight differences between this naïve approach versus our bottom-up model definition.

Model dimensionality

The two-dimensional local model has already been thoroughly studied in [35]. In the non-local case, for a two-dimensional lattice, Eq (10) would read

$$f_j(\mathbf{r}, k+1) = \sum_{m=1}^{\infty} u(\mathbf{r} - m\mathbf{c}_j, k) P_j(\mathbf{r} - m\mathbf{c}_j, k) p_M(m), \tag{15}$$

where $\mathbf{r} \in \mathbb{Z}^2$ is the node position vector, and we have four velocity channels, corresponding to the relative positions of the four nearest neighbors, $\mathbf{c}_1 = (1,0)$, $\mathbf{c}_2 = (0,1)$, $\mathbf{c}_3 = (-1,0)$, and $\mathbf{c}_4 = (0,-1)$, with mean-field channel occupation probabilities

$$P_j(\mathbf{r}, k) = \frac{1}{Z} \exp\left\{\beta \mathbf{c}_j \cdot \sum_{\ell=1}^{4} \mathbf{c}_\ell u(\mathbf{r} + \mathbf{c}_\ell, k)\right\}.$$

Linearizing this equation around the spatially homogeneous steady state $f_n(\mathbf{r}, k) = \frac{\bar{u}}{4}$ (since there are now four velocity channels, each occupied in average by $\bar{f}$ particles) results in

$$f_j(\mathbf{r}, k+1) = \sum_{m=1}^{\infty} \frac{1}{4} p_M(m) \sum_{\ell=1}^{4} f_\ell(\mathbf{r} - m\mathbf{c}_j, k) + \beta \bar{u} \mathbf{c}_j \cdot \sum_{p=1}^{4} \mathbf{c}_p f_\ell(\mathbf{r} - m\mathbf{c}_j + \mathbf{c}_p, k).$$

We now perform a two-dimensional Fourier transform of the system of equations, which again yields a Boltzmann propagator, with entries given by

$$\Gamma_{j,\ell} = \begin{cases} \frac{\phi_M(-q_x)}{4}\left(1 + 2i\beta\bar{u}\sin q_x\right), & j = 1 \\ \frac{\phi_M(-q_y)}{4}\left(1 + 2i\beta\bar{u}\sin q_y\right), & j = 2 \\ \frac{\phi_M(q_x)}{4}\left(1 - 2i\beta\bar{u}\sin q_x\right), & j = 3 \\ \frac{\phi_M(q_y)}{4}\left(1 - 2i\beta\bar{u}\sin q_y\right), & j = 4 \end{cases} \tag{16}$$

where q_x and q_y are the first and second components of the wavevector $\mathbf{q}$, respectively. Again, we find that the propagator entries do not depend on ℓ, and thus it has only one nonzero eigenvalue. It is evident that the Boltzmann propagator for the two-dimensional nonlocal model is completely analogous to the one-dimensional case. Thus, the two-dimensional model can be considered as two one-dimensional models for each spatial dimension. Looking at Eq (13), however, one notices that in the one-dimensional case, there is a factor $\frac{1}{2}$, while in the two-dimensional case, the factor is $\frac{1}{4}$. This is due to the fact that, in one dimension, cells feel a gradient defined only by two neighboring nodes, while in two dimensions, cells sense two times as many nodes to determine the adhesive gradient. In fact, it is straightforward to see that, if cells are able to sense more neighbors, this will only result in a different constant multiplying the second term in the right side of Eqs (13) and (16). The effect of this constant is not a qualitative change in patterns and interactions, but rather, an earlier onset in the order-disorder transition for smaller values of β and $\bar{u}$, since cells can now sense a greater number of cells within more nodes. Simulations of the model in two dimensions can be observed in Fig 4a and 4b. Two-dimensional simulations were performed for a total of 500 time steps, due to computational efficiency. Note that clusters are more defined in the single migration case, as opposed to the block migration case, just as in one dimension, since clusters are more likely to fall apart and reform in the block migration case.

Cell volume exclusion

For simplicity, and due to the high deformability of cancer cells, we have not imposed volume exclusion interactions between cells, thus allowing for the accumulation of cells. There is, however, a physical limit to how many cells a single lattice site may accumulate, even when taking into account that cells may pile up in a three-dimensional arrangement. To take this into account, we could adopt the approach used in a previous study on cancer dynamics [40]: instead of defining the adhesive gradient as done previously, we could use a logistic adhesive gradient defined as

$$G(r,k) = \sum_{j=1}^{2} c_j H\left[u\left(r + c_\ell, k\right)\right],$$

where $H(x)$ is a logistic function

$$H(x) = x\left(1 - \frac{x}{A}\right),$$

where $A>0$ is a new parameter indicating the critical number of cells such that they stop adhering and start repelling one another. With this approach, the homogeneous steady state is still a solution to the discrete mean-field equation. Since we have replaced $u(r,k)$ in the adhesive gradient by $H[u(r,k)]$, we can straightforwardly apply the chain rule, such that the

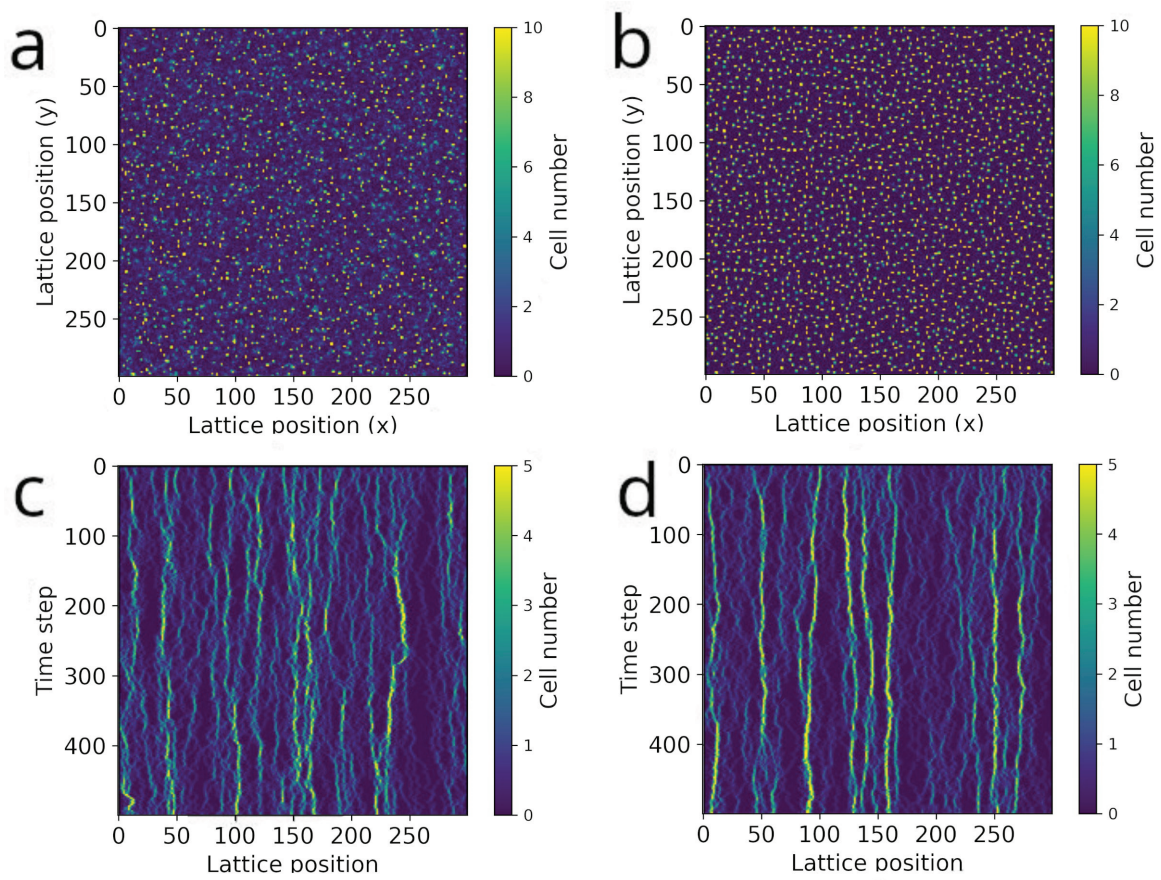

Fig 4. Realizations of two-dimensional and volume exclusion extensions. (a,b): Snapshots of model realizations on two-dimensional space after 500 time steps. The color bar indicates the total number of cells within a node at a given time point. Parameter values were set at $\bar{f} = 0.34$, $\beta = 0.25$, and $s = 5$. Cells migration was either via (a) block migration or (b) cell-wise jumps. (c,d): Kymographs (spatiotemporal plots) of single model realizations with volume exclusion. The color bar indicates the total number of cells at node within a node at a given time point. Parameter values were set at $\bar{f} = 0.34$, $\beta = 0.25$, and $s = 5$. Cells migration was either via (c) block migration or (d) cell-wise jumps.

https://doi.org/10.1371/journal.pcsy.0000048.g004

linearized system is

$$f_j(\mathbf{r}, k+1) = \sum_{m=1}^{\infty} \frac{1}{4} p_M(m) \sum_{\ell=1}^{4} f_\ell(\mathbf{r} - m\mathbf{c}_j, k) + \beta\bar{u}\left(1 - \frac{2\bar{u}}{A}\right)\mathbf{c}_j \cdot \sum_{p=1}^{4} \mathbf{c}_p f_\ell(\mathbf{r} - m\mathbf{c}_j + \mathbf{c}_p, k),$$

where the only difference to the case with no exclusion is the factor $\left(1 - \frac{2\bar{u}}{A}\right)$ accompanying $\beta\bar{u}$. For single-step migration ($M = 1$), the non-trivial eigenvalue takes the form

$$\lambda_2 = \cos(q) + 2\beta\bar{u}\left(1 - \frac{2\bar{u}}{A}\right)\sin^2(q),$$

leading to the instability condition

$$\beta\bar{u}\left(1 - \frac{2\bar{u}}{A}\right) > \frac{1}{4}.$$

When the mean initial density $\bar{u}$ is small, this condition suggests that pattern formation occurs as β increases. However, for large $\bar{u}$, the left-hand side of the inequality can become negative, stabilizing the spatially homogeneous steady state regardless of β. This stabilization arises because high cell densities cause repulsion, preventing aggregation.

The size of the aggregation patterns is also affected. The dominant wavenumber $q_{\max}$, which corresponds to the maximum of the eigenvalue spectrum $\lambda(q)$, determines the pattern wavelength $\Lambda = \frac{2\pi}{q}$. By differentiating Eq (14), we find that the dominant wavenumber for the model without exclusion is

$$q_{\text{ne}} = \arccos\left(\frac{1}{4\beta\bar{u}}\right),$$

while for the model with exclusion, it is

$$q_{\text{e}} = \arccos\left[\frac{1}{4\beta\bar{u}\left(1-\frac{2\bar{u}}{A}\right)}\right].$$

Since $1 - \frac{2\bar{u}}{A} < 1$ for all $\bar{u} > 0$, and the arccosine function is monotonically decreasing, it follows that

$$\Lambda_{\text{e}} > \Lambda_{\text{ne}}.$$

Thus, aggregation patterns in the exclusion model are larger than those in the non-exclusion model.

In the non-local case, the form of the eigenvalues is more complicated, however the predictions are qualitatively similar: no patterns are formed for high $\bar{u}$, and patterns in the exclusion model are larger than in the model without exclusion. Simulations with volume exclusion can be observed in Fig 4c and 4d. Note that, for the same parameter values a with no volume exclusion, cell clusters appear more unstable. This is due to the fact that $\bar{u}\left(1-\frac{2\bar{u}}{A}\right) < \bar{u}$, so for a given density $\bar{u}$, the pattern is less stable.

Limitations of a naïve fractional approach

We have obtained the integro-PDE, Eq (11), bottom-up starting from our cellular automaton model. The resulting equation is markedly different from the local PDE, Eq (7). Naïvely, we could have defined the non-local model by replacing the ordinary derivatives in Eq (7) by fractional derivatives, claiming that such a replacement would take into account the superdiffusive nature of cells. Doing so, would result in the fractional PDE

$$\frac{\partial}{\partial t}u = -D(-\Delta)^s u - \nu\frac{\partial^s}{\partial|x|^s}\left(2uP_2 - u\right), \tag{17}$$

where

$$P_2(x,t) = \frac{1}{2}\exp\left[-2\tilde{\beta}\frac{\partial^s}{\partial|x|^s}u(x,t)\right]\operatorname{sech}\left[2\tilde{\beta}\frac{\partial^s}{\partial|x|^s}u(x,t)\right],$$

and $\frac{\partial^s}{\partial|x|^s}$ is the Riesz fractional derivative. Since both the fractional Laplacian operator and the Riesz fractional derivative are linear, and applying them to a constant yields the zero function, the spatially homogeneous steady state is a solution of this equation. Linearizing around this

solution, and considering that applying the Riesz derivative twice is equivalent to applying the fractional Laplacian operator, we obtain

$$\frac{\partial}{\partial t}u = -(D - 4D\beta\bar{u})(-\Delta)^s u.$$

Using the Fourier transform of the fractional Laplacian,

$$\mathfrak{F}\left\{(-\Delta)^s f(x)\right\}(q) = |q|^{2s}\mathfrak{F}\{f(x)\}(q),$$

we obtain the ordinary differential equation in Fourier space

$$\frac{\mathrm{d}}{\mathrm{d}t}\hat{u}(q,t) = D(4\beta\bar{u} - 1)|q|^{2s}\hat{u}(q,t).$$

Thus, we see that the whole eigenvalue spectrum is negative when $\beta\bar{u} < \frac{1}{4}$ and positive otherwise. This means that, in this naïve fractional model, there is no gradual stabilization of the homogeneous steady state with increasing s, nor is there a dominant eigenvalue resulting in pattern formation, unlike our model.

Discussion

In this paper, we studied an LGCA model of adhesive interacting cells, with Zeta-distributed jump lengths. We considered three migration modes: single-jump (classic) migration, where cells deterministically move by one lattice site every time step, cell-wise cell migration, where cells jump to other lattice sites independently of other cells within the same velocity channel, and block migration, where all cells within the same velocity channel travel to the same node. Mathematically, we derived a conventional, non-linear PDE for the single jump case, as well as a non-linear, non-local, fractional PDE for the block migration case. We found that, in the classic single jump case, cells stop diffusing and start aggregating as soon as either the adhesion sensitivity or the cell density is sufficiently high. Conversely, in the long-jump case, we found that long jumps mainly stabilize the homogeneous steady state, when the distribution tail is sufficiently heavy. Computationally, we found that all models behave qualitatively the same when the probability of performing long jumps decays fast enough. Furthermore, we observe that increasingly probable long jumps gradually inhibit pattern formation. Finally, we found that, for highly adhesive cells and jump distributions with moderately heavy tails, pattern formation is intermittent and patterns appear metastable.

Mathematically, our study has confirmed that, contrary to what some models assume, changing the movement strategy of agents from "diffussive" to "superdiffusive" does not simply result in exchanging local differential operators to non-local operators in the continuous PDE descriptions. In this regard, our observations agree with those found previously by other authors using physical arguments [41]. Indeed, our model shows much richer behavior than the naïve fractional model. Furthermore, our work highlights the potential of agent-based models as bottom-up tools to define novel partial differential equation models, among other macroscopic models[32,42].

Biologically, we have found that highly-adhesive cells can still become invasive as long as they are highly motile, which agrees with experimental observations [43,44]. Furthermore, our simulations show that even if cells seem to form aggregates, these could be metastable

and the aggregate could spontaneously become malignant if cells have a considerable probability to move far away. We can rescale the automaton so that the time step length and lattice sizes reflect experimental obsevations. For example, for B16-F1 cells, by adjusting experimental mean run lengths and mean run times from [14] to the mean jump length and time step length in our model for corresponding parameter values, we obtain that the time step length in our simulations corresponds to approximately 9 minutes, while the length between adjacent nodes should be between 2 to 15 μm. Therefore, our 1000 time step simulations would correspond to about 9000 minutes, or about 6 days, enough time to observe metastable behavior. This could explain the sudden malignancy of apparently benign tumors *in vivo* after xenografting [45]. This observation also agrees with experimental findings which have found that clustering tumor cells are orders of magnitude more efficient in establishing metastases than single cells [46], since several cells could travel together in a single metastable cluster, and spontaneously breaking apart releasing hundreds of cells far away from the main tumor body. Our model could be experimentally tested by using metastatic breast cancer cells, which show Lévy dynamics [14], and regulating their E-cadherin expression, which controls cell-cell adhesivity, and comparing the rate of divergence from a homogeneous initial state, to the model predictions.

Although the model we have proposed in this work has been simplified to ease its mathematical analysis, it can be expanded to account for other types of interaction, volume exclusion effects, correlations between cell velocities during interaction, among others. In the future, we plan to enhance the physical realism of the model by considering superdiffusive behavior originating from non-Markovian time correlations, rather than from power-law jump-length distributions. We also plan to study the qualitative behavior of Eq (11) as well as potential deviations from the LGCA model for different weights of the Zeta distribution tail.

Acknowledgments

The author thanks Andreas Deutsch, Simon Syga, and Alberto Saldaña for fruitful discussions which shaped this paper, and Zuriel Yescas for his input in the integro-PDE model derivation.

Author contributions

Conceptualization: Josué Manik Nava-Sedeño.

Formal analysis: Josué Manik Nava-Sedeño.

Investigation: Josué Manik Nava-Sedeño.

Methodology: Josué Manik Nava-Sedeño.

Software: Josué Manik Nava-Sedeño.

Writing – original draft: Josué Manik Nava-Sedeño.

References

1. Friedl P, Hegerfeldt Y, Tusch M. Collective cell migration in morphogenesis and cancer. Int J Dev Biol. 2004;48(5–6):441–9. https://doi.org/10.1387/ijdb.041821pf PMID: 15349818
2. Ding SS, Muhle LS, Brown AEX, Schumacher LJ, Endres RG. Comparison of solitary and collective foraging strategies of Caenorhabditis elegans in patchy food distributions. Philos Trans R Soc Lond B Biol Sci. 2020;375(1807):20190382. https://doi.org/10.1098/rstb.2019.0382 PMID: 32713303
3. Toret C, Picco A, Boiero-Sanders M, Michelot A, Kaksonen M. The cellular slime mold Fonticula alba forms a dynamic, multicellular collective while feeding on bacteria. Curr Biol. 2022;32(9):1961-1973.e4. https://doi.org/10.1016/j.cub.2022.03.018 PMID: 35349792

4. Gómez-Nava L, Bon R, Peruani F. Intermittent collective motion in sheep results from alternating the role of leader and follower. Nat Phys. 2022;18(12):1494–501.
5. Aguilar J, Zhang T, Qian F, Kingsbury M, McInroe B, Mazouchova N, et al. A review on locomotion robophysics: the study of movement at the intersection of robotics, soft matter and dynamical systems. Rep Prog Phys. 2016;79(11):110001. https://doi.org/10.1088/0034-4885/79/11/110001 PMID: 27652614
6. Liebchen B, Mukhopadhyay AK. Interactions in active colloids. J Phys Condens Matter. 2021;34(8):10.1088/1361-648X/ac3a86. https://doi.org/10.1088/1361-648X/ac3a86 PMID: 34788232
7. Chaté H. Dry aligning dilute active matter. Annu Rev Condens Matter Phys. 2020;11:189–212.
8. Bär M, Großmann R, Heidenreich S, Peruani F. Self-propelled rods: insights and perspectives for active matter. Annu Rev Condens Matter Phys. 2020;11:441–66.
9. Schoeller SF, Holt WV, Keaveny EE. Collective dynamics of sperm cells. Philos Trans R Soc Lond B Biol Sci. 2020;375(1807):20190384. https://doi.org/10.1098/rstb.2019.0384 PMID: 32713305
10. Starruß J, Peruani F, Bär M, Deutsch A. Bacterial swarming driven by rod shape. In: Deutsch A, Brusch L, Byrne H, Vries G, Herzel H, editors. Mathematical modeling of biological systems, volume I: cellular biophysics, regulatory networks, development, biomedicine, and data analysis. Birkhäuser Boston. 2007. p. 163–74.
11. Patel SD, Chen CP, Bahna F, Honig B, Shapiro L. Cadherin-mediated cell-cell adhesion: sticking together as a family. Curr Opin Struct Biol. 2003;13(6):690–8. https://doi.org/10.1016/j.sbi.2003.10.007 PMID: 14675546
12. Kaszak I, Witkowska-Piłaszewicz O, Niewiadomska Z, Dworecka-Kaszak B, Ngosa Toka F, Jurka P. Role of cadherins in cancer-a review. Int J Mol Sci. 2020;21(20):7624. https://doi.org/10.3390/ijms21207624 PMID: 33076339
13. Brabletz T, Kalluri R, Nieto MA, Weinberg RA. EMT in cancer. Nat Rev Cancer. 2018;18(2):128–34. https://doi.org/10.1038/nrc.2017.118 PMID: 29326430
14. Huda S, Weigelin B, Wolf K, Tretiakov KV, Polev K, Wilk G, et al. Lévy-like movement patterns of metastatic cancer cells revealed in microfabricated systems and implicated in vivo. Nat Commun. 2018;9(1):4539. https://doi.org/10.1038/s41467-018-06563-w PMID: 30382086
15. Nousi A, Søgaard MT, Audoin M, Jauffred L. Single-cell tracking reveals super-spreading brain cancer cells with high persistence. Biochem Biophys Rep. 2021;28:101120. https://doi.org/10.1016/j.bbrep.2021.101120 PMID: 34541340
16. Aceto N, Bardia A, Miyamoto DT, Donaldson MC, Wittner BS, Spencer JA, et al. Circulating tumor cell clusters are oligoclonal precursors of breast cancer metastasis. Cell. 2014;158(5):1110–22. https://doi.org/10.1016/j.cell.2014.07.013 PMID: 25171411
17. Macpherson IR, Hooper S, Serrels A, McGarry L, Ozanne BW, Harrington K, et al. p120-catenin is required for the collective invasion of squamous cell carcinoma cells via a phosphorylation-independent mechanism. Oncogene. 2007;26(36):5214–28. https://doi.org/10.1038/sj.onc.1210334 PMID: 17334396
18. Ramis-Conde I, Drasdo D, Anderson ARA, Chaplain MAJ. Modeling the influence of the E-cadherin-beta-catenin pathway in cancer cell invasion: a multiscale approach. Biophys J. 2008;95(1):155–65. https://doi.org/10.1529/biophysj.107.114678 PMID: 18339758
19. Großmann R, Schimansky-Geier L, Romanczuk P. Self-propelled particles with selective attraction–repulsion interaction: from microscopic dynamics to coarse-grained theories. New J Phys. 2013;15(8):085014. https://doi.org/10.1088/1367-2630/15/8/085014
20. Carrillo JA, Colombi A, Scianna M. Adhesion and volume constraints via nonlocal interactions determine cell organisation and migration profiles. J Theor Biol. 2018;445:75–91. https://doi.org/10.1016/j.jtbi.2018.02.022 PMID: 29476831
21. Gutiérrez CMB, Vanhille-Campos C, Alarcón F, Pagonabarraga I, Brito R, Valeriani C. Collective motion of run-and-tumble repulsive and attractive particles in one-dimensional systems. Soft Matter. 2021;17(46):10479–91. https://doi.org/10.1039/d1sm01006a PMID: 34750600
22. Caprini L, Löwen H. Flocking without alignment interactions in attractive active Brownian particles. Phys Rev Lett. 2023;130(14):148202. https://doi.org/10.1103/PhysRevLett.130.148202 PMID: 37084461
23. Cairoli A, Lee C. Hydrodynamics of active Lévy matter. arXiv preprint. 2019. https://arxiv.org/abs/1903.07565
24. Großmann R, Peruani F, Bär M. Superdiffusion, large-scale synchronization, and topological defects. Phys Rev E. 2016;93:040102. https://doi.org/10.1103/PhysRevE.93.040102 PMID: 27176235

25. Estrada-Rodriguez G, Gimperlein H. Interacting particles with Lévy strategies: limits of transport equations for swarm robotic systems. SIAM J Appl Math. 2020;80(1):476–98. https://doi.org/10.1137/18m1205327
26. Zhou T, Peng Z, Gulian M, Brady J. Distribution and pressure of active Lévy swimmers under confinement. J Phys A-Math Theor. 2021;54(27):275002.
27. Dipierro S, Giacomin G, Valdinoci E. The Lévy flight foraging hypothesis: comparison between stationary distributions and anomalous diffusion. J Phys A-Math Theor. 2023;56(48):485601.
28. Daus ES, Ptashnyk M, Raithel C. Derivation of a fractional cross-diffusion system as the limit of a stochastic many-particle system driven by Lévy noise. J Diff Eq. 2022;309:386–426. https://doi.org/10.1016/j.jde.2021.11.027
29. Estrada-Rodriguez G, Lorenzi T. Macroscopic limit of a kinetic model describing the switch in T cell migration modes via binary interactions. Eur J Appl Math. 2023;34(1):1–27.
30. Iqbal N, Wu R, Liu B. Pattern formation by super-diffusion in FitzHugh–Nagumo model. Appl Math Comput. 2017;313:245–58.
31. Deutsch A, Nava-Sedeño JM, Syga S, Hatzikirou H. BIO-LGCA: A cellular automaton modelling class for analysing collective cell migration. PLoS Comput Biol. 2021;17(6):e1009066. https://doi.org/10.1371/journal.pcbi.1009066 PMID: 34129639
32. Nava-Sedeño JM, Hatzikirou H, Voß-Böhme A, Brusch L, Deutsch A, Peruani F. Vectorial active matter on the lattice: polar condensates and nematic filaments. New J Phys. 2023;25(12):123046. https://doi.org/10.1088/1367-2630/ad1498
33. Harris TH, Banigan EJ, Christian DA, Konradt C, Tait Wojno ED, Norose K, et al. Generalized Lévy walks and the role of chemokines in migration of effector CD8+ T cells. Nature. 2012;486(7404):545–8. https://doi.org/10.1038/nature11098 PMID: 22722867
34. Passucci G, Brasch ME, Henderson JH, Zaburdaev V, Manning ML. Identifying the mechanism for superdiffusivity in mouse fibroblast motility. PLoS Comput Biol. 2019;15(2):e1006732. https://doi.org/10.1371/journal.pcbi.1006732 PMID: 30763309
35. Deutsch A, Dormann S. Cellular automaton modeling of biological pattern formation: characterization, examples, and analysis. 2nd edn. Birkhäuser. 2018.
36. Syga S. Impacts of genetic and phenotypic heterogeneity on tumor evolution: mathematical modeling and analysis. Technische Universität Dresden. 2024. https://nbn-resolving.org/urn:nbn:de:bsz:14-qucosa2-898257
37. Abatangelo N, Valdinoci E. Getting acquainted with the fractional laplacian. In: Dipierro S, editor. Contemporary research in elliptic pdes and related topics. Cham: Springer. 2019. p. 1–105.
38. Di Nezza E, Palatucci G, Valdinoci E. Hitchhikers guide to the fractional Sobolev spaces. Boll Sci Math. 2012;136(5):521–73.
39. Nava-Sedeño JM, Syga S, Deutsch A. Artificial patterns in spatially discrete models of cell migration and how to mitigate them. BIOMATH. 2023;12(2):2311177. https://doi.org/10.55630/j.biomath.2023.11.177
40. Ilina O, Gritsenko PG, Syga S, Lippoldt J, La Porta CAM, Chepizhko O, et al. Cell-cell adhesion and 3D matrix confinement determine jamming transitions in breast cancer invasion. Nat Cell Biol. 2020;22(9):1103–15. https://doi.org/10.1038/s41556-020-0552-6 PMID: 32839548
41. Cairoli A, Klages R, Baule A. Weak Galilean invariance as a selection principle for coarse-grained diffusive models. Proc Natl Acad Sci U S A. 2018;115(22):5714–9. https://doi.org/10.1073/pnas.1717292115 PMID: 29760057
42. Pillay S, Byrne HM, Maini PK. Modeling angiogenesis: a discrete to continuum description. Phys Rev E. 2017;95(1):012410. https://doi.org/10.1103/PhysRevE.95.012410 PMID: 28208423
43. Räsänen K, Vaheri A. TGF-beta1 causes epithelial-mesenchymal transition in HaCaT derivatives, but induces expression of COX-2 and migration only in benign, not in malignant keratinocytes. J Dermatol Sci. 2010;58(2):97–104. https://doi.org/10.1016/j.jdermsci.2010.03.002 PMID: 20399617
44. Rodriguez FJ, Lewis-Tuffin LJ, Anastasiadis PZ. E-cadherin's dark side: possible role in tumor progression. Biochim Biophys Acta. 2012;1826(1):23–31. https://doi.org/10.1016/j.bbcan.2012.03.002 PMID: 22440943
45. Sordat B. From ectopic to orthotopic tumor grafting sites: evidence for a critical role of the host tissue microenvironment for the actual expression of the malignant phenotype. In: Hoffman R, editor. Patient-derived mouse models of cancer: patient-derived orthotopic xenografts (PDOX). Cham: Humana Press. 2017. p. 43–53.
46. Stuelten CH, Parent CA, Montell DJ. Cell motility in cancer invasion and metastasis: insights from simple model organisms. Nat Rev Cancer. 2018;18(5):296–312. https://doi.org/10.1038/nrc.2018.15 PMID: 29546880